PHOTONICS Research

Optical vortex copier and regenerator in the Fourier domain

Xiaodong Qiu,[1] Fangshu Li,[1] Haigang Liu,[2] Xianfeng Chen,[2,3] and Lixiang Chen[1,4]

[1]Department of Physics, Jiujiang Research Institute and Collaborative Innovation Center for Optoelectronic Semiconductors and Efficient Devices, Xiamen University, Xiamen 361005, China
[2]State Key Laboratory of Advanced Optical Communication Systems and Networks, School of Physics and Astronomy, Shanghai Jiao Tong University, Shanghai 200240, China
[3]e-mail: xfchen@sjtu.edu.cn
[4]e-mail: chenlx@xmu.edu.cn

Received 12 January 2018; revised 22 March 2018; accepted 5 April 2018; posted 12 April 2018 (Doc. ID 319681); published 24 May 2018

The generation and manipulation of optical vortices are of fundamental importance in a variety of promising applications. Here, we develop a nonlinear optical paradigm to implement self- and cross-convolution of optical vortex arrays, demonstrating the features of a vortex copier and regenerator. We use a phase-only spatial light modulator to prepare the 1064 nm invisible fundamental light to carry special optical vortex arrays and use a potassium titanyl phosphate crystal to perform type II second-harmonic generation in the Fourier domain to achieve 532 nm visible structured vortices. Based on pure cross-convolution, we succeed in copying arbitrary-order single vortices as well as their superposition states onto a prearranged array of fundamental Gaussian spots. Also, based on the simultaneous effect of self- and cross-convolutions, we can expand the initial vortex lattices to regenerate more vortices carrying various higher topological charges. Our presented method of realizing an optical vortex copier and regenerator could find direct applications in optical manipulation, optical imaging, optical communication, and quantum information processing with structured vortex arrays.

OCIS codes: (050.4865) Optical vortices; (190.2620) Harmonic generation and mixing; (070.4340) Nonlinear optical signal processing.

https://doi.org/10.1364/PRJ.6.000641

1. INTRODUCTION

An optical vortex is distinguished by an undefined phase point with zero amplitude in the wave front, i.e., phase singularity, around which the phase varies azimuthally by a nonzero integer multiple of 2π [1]. The simplest case of an optical vortex is the twisted light beam with a helical phase, $\exp(il\varphi)$, with l being an integer and φ the azimuthal angle, and within such a light beam each photon carries a well-defined orbital angular momentum of $l\hbar$ [2]. Recent years have witnessed a growing interest in various applications with optical vortex or orbital angular momentum, including optical tweezers and spanners, optical communications, high-dimensional quantum entanglement, and quantum information protocols [3–6]. Until now, several mature techniques have been invented to produce optical vortices, including $\pi/2$ mode converter [7], spiral phase plate [8], Q-plate [9], well-defined integrated optoelectronics [10], commercial spatial light modulator (SLM) [11], etc.

Compared with the single or isolated optical vortex, the network of vortices, i.e., optical vortex array [12,13], is of significant importance in certain fields. As optical vortices contain abundant information from scattered objects, they were exploited as a sensing technique for digital spiral imaging [14,15]. Owing to its specific structural features, an optical vortex array has dramatically promoted the developments of optical metrology [16], optical communication [17], microlithography [18], and multiple optical traps for rapidly assembling or guiding particulates [19] and detection at a very low light level [20]. Similarly, an optical vortex array of any desired structure could be generated and manipulated with computer-generated holograms displayed by SLM [21]. Also, multibeam interference, e.g., using superpositions of several plane waves, spherical waves, or Hermite–Gaussian beams was another effective way to generate optical vortex arrays [22–24]. Based on a single topological defect in a nematic liquid crystal mesophase, generation of tunable structured light fields endowed with various sets of phase singularities was reported [25–27]. Besides, an energy equal optical vortex array with an arbitrary topological charge was achieved by specially designing a Dammann vortex grating [28]. We note that the above schemes are merely implemented within the frame of linear optics,

whereas the nonlinear optical methods, e.g., second-harmonic generation (SHG) [29–32], parametric downconversion [4,33–35], stimulated Brillouin amplification [36], and wave mixing in a Kerr-like nonlinear medium [37], have also been explored to generate a single optical vortex with frequency conversion. In particular, twisted nonlinear photonic crystals with spatially structured nonlinear susceptibility were recently reported to efficiently generate an optical vortex array [38]. One fascinating application with the nonlinear method is its role serving as a bridge to transfer information between two vortex-based quantum networks that employ different wavelengths [39]. We also note that the above linear and nonlinear schemes were implemented in the real space only, while not yet exploring the features endowed by Fourier optics. Here, we conduct such an experiment to perform SHG with a potassium titanyl phosphate (KTP) crystal in the Fourier domain with structured optical vortex arrays and reveal the interesting effects of self- and cross-convolution between the constituent vortices. Of particular interest is the demonstration of two functions and features achieved by our configurations, which we term "optical vortex copier and regenerator." The experimental observations are in excellent agreement with our theoretical analysis.

2. OPTICAL VORTEX COPIER

We sketch our experimental setup of an optical vortex copier in Fig. 1. A laser-diode-pumped all-solid-state 1064 nm laser (Cobolt, Rumba) serves as the invisible illumination source. After being collimated and expanded by a telescope, the linear polarized 1064 nm light is incident on a computer-controlled SLM (Hamamatsu, X10468-07). The SLM is a reflective device that consists of an array of pixels (792 × 600) with an effective area of 16 mm × 12 mm and a pixel pitch of 20 μm. Each pixel individually imprints the incoming light with a phase modulation ($0 \sim 2\pi$) according to the 8 bit gray-scale ($0 \sim 255$). Here, we divide the whole pixel array into two subdomains, each of which individually displays a specially designed holographic grating to produce the desired optical vortex array. For this, we first add a blazed grating modulo 2π to the phase profile of the desired vortex array; then, we obtain a pure-phase holographic grating. Subsequently, we multiply the phase grating with the desired intensity distribution to obtain the final hologram, which is displayed by SLM.

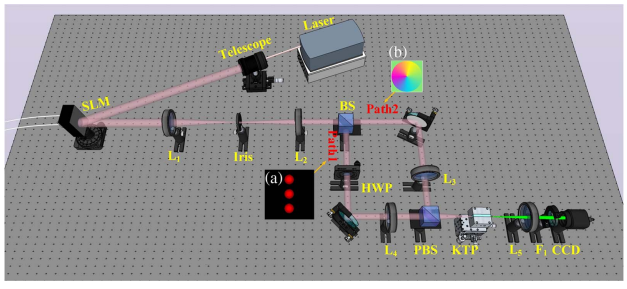

Fig. 1. Schematic overview of experimental setup to realize the optical vortex copier via type-II second-harmonic generation in the Fourier domain (see the text for details). Insets (a) and (b) show the initial array of Gaussian spots in Path 1 and the single vortex in Path 2, respectively.

By an optical $4f$ system consisting of two lenses ($f_1 = 750$ mm and $f_2 = 250$ mm) and an adjustable iris, we select the first-order diffracted lights reflected from SLM, which carry the desired optical vortex arrays.

We assume that the vortex arrays in Path 1 and Path 2 can be, respectively, described as

$$E_1(r,\phi) = \sum_i A_{1,i}(r_i)\exp(il_i\phi_i), \tag{1}$$

$$E_2(r,\phi) = \sum_j A_{2,j}(r_j)\exp(il_j\phi_j). \tag{2}$$

Note that each vortex in both paths is defined at its own circular coordinates (r_i,ϕ_i) and (r_j,ϕ_j) with respect to the individual center. The subscripts i and j denote the i-th and j-th vortex of topological charge l_i and l_j in Path 1 and Path 2, respectively. Here, we adopt the Laguerre–Gaussian (LG) modes [2] with zero radial index $p = 0$ to describe the amplitude of each vortex, namely, $A_{1,i}(r_i) = \sqrt{\frac{2}{\pi w^2 |l_i|!}}\left(\frac{\sqrt{2}r_i}{w}\right)^{|l_i|}\exp\left(-\frac{r_i^2}{w^2}\right)$, where w is the beam waist, and $A_{2,j}(r_j)$ is defined in the same way. In each path, we use a lens (L_3 or L_4, $f_3 = f_4 = 100$ mm) to perform the Fourier transform on the input initial vortex array [Eq. (1) or Eq. (2)], namely, $\tilde{E}_1(\rho,\varphi) = \sum_i \mathcal{F}[A_{1,i}(r_i)\exp(il_i\phi_i)]$ and $\tilde{E}_2(\rho,\varphi) = \sum_j \mathcal{F}[A_{2,j}(r_j)\exp(il_j\phi_j)]$. By a polarizing beam splitter (PBS), we recombine two paths and then superpose their Fourier spectra at the common Fourier plane where the KTP crystal is placed. As the KTP is cut for type-II phase matching, we insert into Path 2 an additional half-wave plate (HWP) with its fast axis orienting at 45° in order to rotate the vertical polarization into the horizontal one. Thus, these two Fourier spectra, $\tilde{E}_1(\rho,\varphi)$ and $\tilde{E}_2(\rho,\varphi)$, serving as the fundamental lights, participate in the SHG process together. Under the paraxial approximation and phase-matching condition, the SHG light field can be described by the following coupled equation [40]

$$\frac{\mathrm{d}\tilde{E}_3(\rho,\varphi)}{\mathrm{d}z} = \frac{i\omega_3^2 d_{\mathrm{eff}}}{k_3 c^2}\tilde{E}_1(\rho,\varphi)\tilde{E}_2(\rho,\varphi), \tag{3}$$

where d_{eff} is the effective nonlinear coefficient, z is the propagation distance, and ω_3 and k_3 are the frequency and wave vector of SHG wave, respectively. The subsequent lens 5 (L_5) undoes the Fourier transform on the SHG wave described by Eq. (3). By considering the small-signal approximation, we derive the output light field as

$$\begin{aligned} E_3(r,\phi) &= \alpha\mathcal{F}[\tilde{E}_1(\rho,\phi)\tilde{E}_2(\rho,\phi)] \\ &= \alpha\sum_{ij}[A_{1,i}(r_i)\exp(il_i\phi_i)] * [A_{2,j}(r_j)\exp(il_j\phi_j)], \end{aligned} \tag{4}$$

where $\alpha = i\omega_3^2 d_{\mathrm{eff}} L/k_3 c^2$ with L being the crystal length, and $*$ denotes the convolution operation. After filtering out 532 nm SHG light fields by the filter F_1, we use a color CCD camera (Thorlabs, DCU224C) to record the resultant optical patterns at the rear focal plane of L_5. It is shown by Eq. (4) that our configuration enables the cross-convolutional computation between two vortex arrays via SHG in the Fourier domain.

By utilizing the Fourier transform of the LG modes [41], we can derive that

$$[A_{1,i}(r_i)\exp(il_i\phi_i)]*[A_{2,j}(r_j)\exp(il_j\phi_j)]$$
$$=\mathcal{F}^{-1}\{\mathcal{F}[A_{1,i}(r_i)\exp(il_i\phi_i)]\times\mathcal{F}[A_{2,j}(r_j)\exp(il_j\phi_j)]\}$$
$$=\sqrt{\frac{2}{\pi w^2(|l_i+l_j|)!}}\left(\frac{\sqrt{2}r}{w}\right)^{|l_i+l_j|}\exp\left(-\frac{r^2}{w^2}\right)\exp[i(l_i+l_j)\phi], \quad (5)$$

which reveals clearly that the convolution of every two vortices results in a new vortex with its topological charge appearing as a sum of the former two. To realize the function of the optical vortex copier, we prepare the initial array, which merely consists of several fundamental Gaussian spots in Path 1, i.e., $l_i = 0$, while in Path 2 we make the single vortices as well as their superposition states. Without loss of the generality, we make $E_2(r,\phi) = A_2(r)\exp(il\phi)$ to bear only a single vortex of topological charge l; then, according to Eq. (5), we can simplify Eq. (4) to $E_3(r,\phi) \propto \sum_i A_{3,i}(r_i)\exp(il\phi_i)$, which reveals that we can copy the vortex states in Path 2 onto the resultant SHG light fields, while acquiring the array structure of Path 1, just like a copier. The same algorithm can be applied to the case of the collinear superpositions of two vortices. We show our experimental results in Fig. 2.

We prepare a line of three Gaussian spots in Path 1 [see Fig. 2(a)]. While in Path 2, we prepare two single vortices with topological charges of $l = 1$ and $l = 2$, respectively [see the insets of Figs. 2(b) and 2(c)]. We can see from Figs. 2(b) and 2(c) that we have succeeded in copying the target vortex onto the resultant SHG light fields, while maintaining the initial line structure. Namely, a line of three single vortices with $l = 1$ and that of three vortices with $l = 2$ are generated, respectively. Besides, the topological charges of $l = 1$ and 2 can be distinguished intuitively from the dark cores, as they generally scale with $\sqrt{|l|}$ [42]. We also consider another case of collinear superpositions of two vortices with opposite topological charges. The initial Gaussian spots in Path 1 are prepared in a pentagonal array [see Fig. 2(d)]. The vortex superpositions in Path 2 are $l = \pm 1$ and $l = \pm 2$, respectively [see the insets of Figs. 2(e) and 2(f)]. We can see that we have successfully copied the target superposition states onto the pentagonal arrays, resulting in the SHG light fields of pentagonal petal-like patterns. Due to the azimuthal constructive and destructive interference between two opposite vortices, we also verify that the petal number equals $2|l|$ [11,43]. In other words, based on the cross-convolution between an initial Gaussian spot array and a variety of vortex states, we have demonstrated the function and feature of our optical vortex copier.

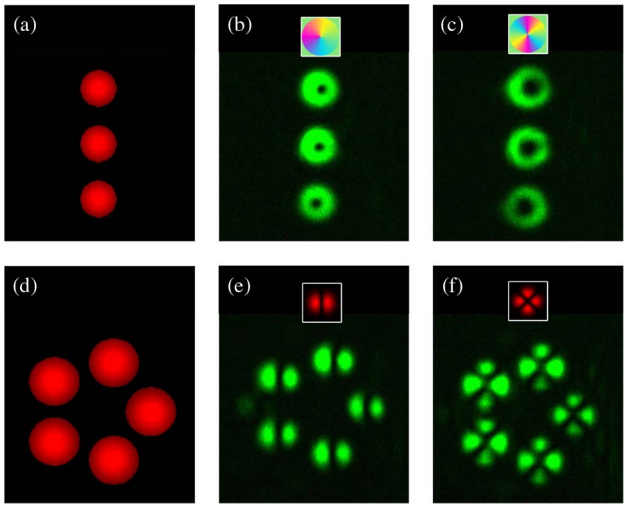

Fig. 2. Experimental observations of the optical vortex copier. (a) and (d) Initial structured arrays of fundamental Gaussian spots. Single vortex with (b) $l = 1$ and (c) $l = 2$. Superposition of two vortices with (e) $l = \pm 1$ and (f) $l = \pm 2$.

3. OPTICAL VORTEX REGENERATOR

In contrast with the cross-convolution-based optical vortex copier, here we aim to demonstrate the optical vortex regenerator based on the self-convolution of an arbitrary vortex array. For this, the experimental setup is rearranged and sketched in Fig. 3. We make the fundamental lights carry the same vortex arrays, and one key step is to use an additional half-wave plate with its fast axis orienting at 22.5° to make the polarization pose at 45°. As a result, the horizontal and vertical components with identical spatial profile, i.e., $E_1(r,\phi) = E_2(r,\phi)$, in Eqs. (1) and (2), can satisfy the type-II phase matching condition and participate in the SHG collinearly in the KTP crystal. Accordingly, we need to rewrite Eq. (4) as

$$E_3(r,\phi) \propto \sum_i [A_{1,i}(r_i)\exp(il_i\phi_i)]*[A_{1,i}(r_i)\exp(il_i\phi_i)]$$
$$+\sum_{i\neq j}[A_{1,i}(r_i)\exp(il_i\phi_i)]*[A_{1,j}(r_j)\exp(il_j\phi_j)]. \quad (6)$$

It is clearly revealed by Eq. (6) that the self-convolution of an arbitrary array can be considered as the self-convolution of each constituent vortex and the cross-convolution between every two different vortices. For example, if we prepare the initial array of two single vortices with topological charges, l_1 and l_2, as marked as A and B in inset (a) of Fig. 3, then, after SHG, we obtain the output array of three single vortices, as a result of both self- and cross-convolution, namely, A ∗ A, A ∗ B, and B ∗ B, accompanying with the increase of topological charges as $l_1' = 2l_1$, $l_2' = l_1 + l_2$, and $l_3' = 2l_2$, respectively. In other

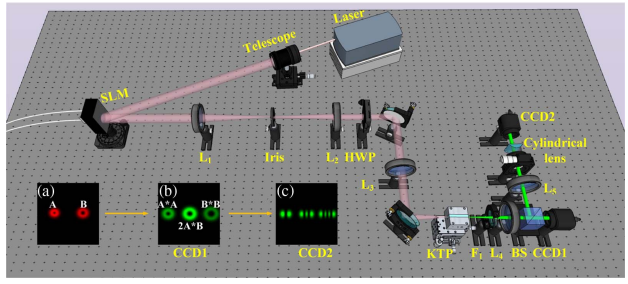

Fig. 3. Schematic overview of the experimental setup to realize the optical regenerator (see the text for details). Insets (a), (b), and (c) show the initial array of two single vortices, the corresponding results of self-convolution, and the resultant array after the cylindrical lens, respectively.

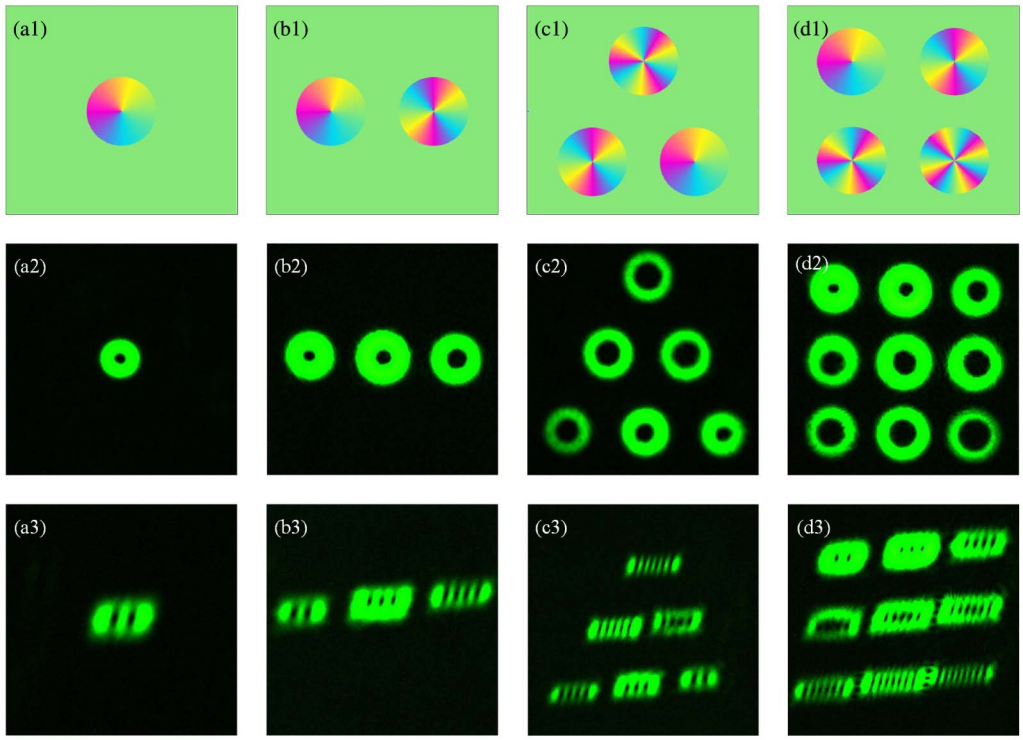

Fig. 4. Experimental observations of the optical vortex regenerator with different arrays of single vortices. Top panel: Initial input arrays encoded in 1064 nm fundamental lights. Middle: Regenerated arrays encoded in 532 nm SHG light fields. Bottom: Measurements of topological charges with a cylindrical lens.

words, we can realize the optical vortex regenerator, which is able to regenerate more vortices with higher topological chargers from an initial low-order vortex array; therefore, the initial array is expanded.

The experimental results are presented in Fig. 4. We prepare the initial arrays of a single vortex, two vortices, triangle vortices, and quadrangular vortices, respectively (see the top panel in Fig. 4). After the SHG in the Fourier domain, we obtain the output arrays that consist of more vortices (see the middle panel). For a single vortex of $l = 1$, we merely obtain a single vortex whose topological charge is trivially doubled, i.e., $l' = 2$. For two single vortices of $l_1 = 1$ and $l_2 = 2$, as mentioned above, we have three newly regenerated vortices whose topological charges are $l'_1 = 2$, $l'_2 = 3$, and $l'_3 = 4$, respectively. For the triangular case, the three vortices at each vertex result from the self-convolution of each input vortex, taking topological charges $l'_1 = 6$, $l'_2 = 4$, and $l'_3 = 2$, respectively. While the other three at the middle of each side originate from the cross-convolution between every two of input vortices, taking $l'_4 = 5$, $l'_5 = 4$, and $l'_6 = 2$, respectively. Similarly, for the 2×2 input array, we can reproduce an expanded 3×3 output array, as shown in Fig. 4. The four vertex vortices are produced from self-convolution with doubled topological charges, while the other five are generated from cross-convolution.

In order to determine the topological charges of each newly regenerated optical vortex, we adopt a single cylindrical lens [44,45] to convert the vortex beams described by $\mathrm{LG}^{l}_{p=0}$ into 1D horizontal lattices, with the lobe number N characterized by $N = l + 1$. After the cylindrical converter, we record the resultant optical patterns with the color CCD camera. As shown in the bottom panel of Fig. 4, we can see that the helical phase of each doughnut-shaped vortex is unfolded, changing into the characteristic 1D optical lattices, which give us directly the information of topological charge according to the relation of $N = l + 1$. We take the quadrangular case in Fig. 4, for example, which initially has a 2×2 vortex array with $l = 1$, 2, 3, 4, respectively (left to right, top to bottom). After simultaneous self- and cross-convolution, we have the output-expanded 3×3 vortex array. By observing the lobe numbers of 1D lattices in the bottom panel, we deduce that the generated topological charges are $l = 2$, 3, 4; 4, 5, 6; and 6, 7, 8, respectively (left to right, top to bottom).

We further perform another experiment of optical vortex regenerator with an array of coherent superposition states of vortex beams. As is shown by Fig. 5(a), the initial input array is composed of five different superposition states, namely, $\mathrm{LG}^{4}_{0} + \mathrm{LG}^{-4}_{0}$, $\mathrm{LG}^{2}_{0} + \mathrm{LG}^{-2}_{0}$, $\mathrm{LG}^{0}_{0} + \mathrm{LG}^{0}_{0}$, $\mathrm{LG}^{3}_{0} + \mathrm{LG}^{-3}_{0}$, and $\mathrm{LG}^{1}_{0} + \mathrm{LG}^{-1}_{0}$, respectively, with the petal number specified as $2|l|$. We present our experimental observations in Fig. 5(b), from which we can see that more new superposition states can be generated, and the array is expanded effectively, as a consequence of both self- and cross-convolutions between the constituent vortices. In light of Eq. (6), we conclude that the pattern on the top right corner, marked with the white box in Fig. 5(b), is generated from the self-convolution of the input superposition state, $\mathrm{LG}^{2}_{0} + \mathrm{LG}^{-2}_{0}$, in Fig. 5(a). Thus, it can be described by the following coherent superposition, $\mathrm{LG}^{4}_{0} + 2\mathrm{LG}^{0}_{0} + \mathrm{LG}^{-4}_{0}$, leading to nine maxima in the output

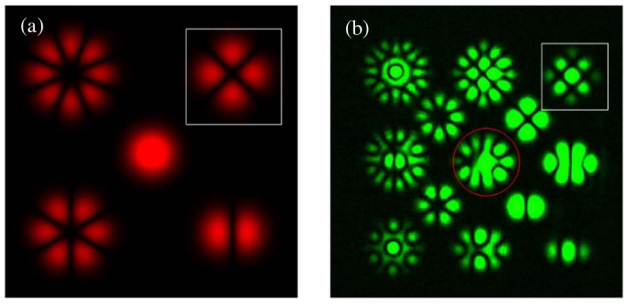

Fig. 5. Experimental observations of the optical vortex regenerator with an array of vortex superposition states. (a) Numerical simulation of input array. (b) Output array.

intensity pattern. In contrast, the generation of the central pattern in Fig. 5(b), marked by the red circle, is a bit more complicated. Its formation has threefold contributions, i.e., one self-convolution and two cross-convolutions between the constituent vortices in Fig. 5(a). Specifically, the self-convolution of the central one still results in a Gaussian spot described by LG_0^0. While the cross-convolution between two diagonal vertices produces the superposition, $\mathrm{LG}_0^5+\mathrm{LG}_0^3+\mathrm{LG}_0^{-3}+\mathrm{LG}_0^{-5}$, the convolution between two antidiagonal vertices generates the superposition, $\mathrm{LG}_0^5+\mathrm{LG}_0^1+\mathrm{LG}_0^{-1}+\mathrm{LG}_0^{-5}$. Thus, we know that the newly generated central pattern in Fig. 5(b) is mathematically corresponding to the coherent superposition, $2\mathrm{LG}_0^5+\mathrm{LG}_0^3+\mathrm{LG}_0^1+\mathrm{LG}_0^0+\mathrm{LG}_0^{-1}+\mathrm{LG}_0^{-3}+2\mathrm{LG}_0^{-5}$, which is in essence a multilevel orbital angular momentum state in a high-dimensional Hilbert space [46]. In other words, our present scheme of an optical vortex regenerator offers a feasible technique to generate more high-order vortices as well as their superposition states with a specially designed structure.

4. CONCLUSION

In summary, we proposed and conducted the SHG experiment with optical vortex arrays in the Fourier domain, in contrast with previous work considering only single vortices in the real domain. Based on a cross-convolution configuration, we succeeded in copying the target single vortices as well as their superposition states onto a prearranged array of Gaussian spots. Besides, based on simultaneous self- and cross-convolution, we realized the optical vortex regenerator that can generate more vortices of higher topological charges, even their various superposition states of a specially designed structure. It is noted that the number of vortices and their superpositions in the array is limited by the crystal's acceptance angle, which is related to the phase-matching condition as well as the crystal length. By adopting a more effective nonlinear crystal or system to enable strong photon–photon interaction, our method could potentially be extended to the few-photon level. Our present work may find potential applications in the fields of optical micromanipulation, free-space optical communication with vortex multiplexing, and quantum information protocols with high-dimensional orbital angular momentum states.

Funding. National Natural Science Foundation of China (NSFC) (11474238, 11734011, 91636109); Fundamental Research Funds for the Central Universities at Xiamen University (20720160040); Natural Science Foundation of Fujian Province (2015J06002); Program for New Century Excellent Talents in University (NCET) (NCET-13-0495); National Key R&D Program of China (2017YFA0303700).

REFERENCES

1. G. J. Ruane, G. A. Swartzlander, S. Slussarenko, L. Marrucci, and M. R. Dennis, "Nodal areas in coherent beams," Optica **2**, 147–150 (2015).
2. L. Allen, M. W. Beijersbergen, R. J. C. Spreeuw, and J. P. Woerdma, "Orbital angular momentum of light and the transformation of Laguerre-Gaussian laser modes," Phys. Rev. A **45**, 8185–8189 (1992).
3. S. Franke-Arnold, L. Allen, and M. Padgett, "Advances in optical angular momentum," Laser Photon. Rev. **2**, 299–313 (2008).
4. G. Molina-Terriza, J. P. Torres, and L. Torner, "Twisted photons," Nat. Phys. **3**, 305–310 (2007).
5. A. M. Yao and M. J. Padgett, "Orbital angular momentum: origins, behavior and applications," Adv. Opt. Photon. **3**, 161–204 (2011).
6. M. R. Dennis, K. O'Holleran, and M. J. Padgett, "Singular optics: optical vortices and polarization singularities," Prog. Opt. **53**, 293–363 (2009).
7. D. Naidoo, F. S. Roux, A. Dudley, I. Litvin, B. Piccirillo, L. Marrucci, and A. Forbes, "Controlled generation of higher-order Poincaré sphere beams from a laser," Nat. Photonics **10**, 327–332 (2016).
8. M. W. Beijersbergen, R. P. C. Coewinkel, M. Kristensen, and J. P. Woerdman, "Helical-wavefront laser beams produced with a spiral phase plate," Opt. Commun. **112**, 321–327 (1994).
9. S. Slussarenko, A. Murauski, T. Du, V. Chigrinov, L. Marrucci, and E. Santamato, "Tunable liquid crystal q-plates with arbitrary topological charge," Opt. Express **19**, 4085–4090 (2011).
10. X. Cai, J. Wang, M. J. Strain, B. Johnson-Morris, J. Zhu, M. Sorel, J. L. O'Brien, M. G. Thompson, and S. Yu, "Integrated compact optical vortex beam emitters," Science **338**, 363–366 (2012).
11. L. Chen, W. Zhang, Q. Lu, and X. Lin, "Making and identifying optical superpositions of high orbital angular momenta," Phys. Rev. A **88**, 053831 (2013).
12. D. Rozas, Z. S. Sacks, and G. A. Swartzlander, "Experimental observation of fluidlike motion of optical vortices," Phys. Rev. Lett. **79**, 3399–3402 (1997).
13. I. Maleev and G. Swartzlander, "Composite optical vortices," J. Opt. Soc. Am. B **20**, 1169–1176 (2003).
14. L. Torner, J. P. Torres, and S. Carrasco, "Digital spiral imaging," Opt. Express **13**, 873–881 (2005).
15. L. Chen, J. Lei, and J. Romero, "Quantum digital spiral imaging," Light Sci. Appl. **3**, e153 (2014).
16. W. Wang, T. Yokozeki, R. Ishijima, M. Takeda, and S. G. Hanson, "Optical vortex metrology based on the core structures of phase singularities in Laguerre-Gauss transform of a speckle pattern," Opt. Express **14**, 10195–10206 (2006).
17. G. Gibson, J. Courtial, M. Padgett, M. Vasnetsov, V. Pasko, S. M. Barnett, and S. Franke-Arnold, "Free-space information transfer using light beams carrying orbital angular momentum," Opt. Express **12**, 5448–5456 (2004).
18. M. D. Levenson, T. J. Ebihara, G. Dai, Y. Morikawa, N. Hayashi, and S. M. Tan, "Optical vortex mask via levels," J. Microlithogr. Microfabr. Microsyst. **3**, 293–304 (2004).
19. K. Ladavac and D. Grier, "Microoptomechanical pumps assembled and driven by holographic optical cortex arrays," Opt. Express **12**, 1144–1149 (2004).
20. W. Zhang, J. Wang, F. Li, L. Chen, and E. Karimi, "Revealing optical vortices with a small number of photons," Laser Photon. Rev. **11**, 1600163 (2017).
21. J. E. Curtis, B. A. Koss, and D. G. Grier, "Dynamic holographic optical tweezers," Opt. Commun. **207**, 169–175 (2002).
22. J. Masajada and B. Dubik, "Optical vortex generation by three plane wave interference," Opt. Commun. **198**, 21–27 (2001).

23. S. Vyas and P. Senthilkumaran, "Vortex array generation by interference of spherical waves," Appl. Opt. **46**, 7862–7867 (2007).
24. Y. C. Lin, T. H. Lu, K. F. Huang, and Y. F. Chen, "Generation of optical vortex array with transformation of standing-wave Laguerre-Gaussian mode," Opt. Express **19**, 10293–10303 (2011).
25. E. Brasselet, "Tunable optical vortex arrays from a single nematic topological defect," Phys. Rev. Lett. **108**, 087801 (2012).
26. R. Barboza, U. Bortolozzo, M. G. Clerc, S. Residori, and E. Vidal-Henriquez, "Optical vortex induction via light-matter interaction in liquid-crystal media," Phys. Rev. Lett. **111**, 093902 (2013).
27. R. Barboza, U. Bortolozzo, M. G. Clerc, G. Assanto, E. Vidal-Henriquez, and S. Residori, "Harnessing optical vortex lattices in nematic liquid crystals," Adv. Opt. Photon. **7**, 635–683 (2015).
28. P. Chen, S. Ge, L. Ma, W. Hu, V. Chigrinov, and Y. Lu, "Generation of equal-energy orbital angular momentum beams via photopatterned liquid crystals," Phys. Rev. Appl. **5**, 044009 (2016).
29. Z. Zhou, D. Ding, Y. Jiang, Y. Li, S. Shi, X. Wang, and B. Shi, "Orbital angular momentum light frequency conversion and interference with quasi-phase matching crystals," Opt. Express **22**, 20298–20310 (2014).
30. K. Dholakia, N. B. Simpson, M. J. Padgett, and L. Allen, "Second-harmonic generation and the orbital angular momentum of light," Phys. Rev. A **54**, R3742–R3745 (1996).
31. W. T. Buono, L. F. C. Moraes, J. A. O. Huguenin, C. F. R. Souza, and A. Z. Khoury, "Arbitrary orbital angular momentum addition in second harmonic generation," New J. Phys. **16**, 093041 (2014).
32. L. J. Pereira, W. T. Buono, D. S. Tasca, K. Dechoum, and A. Z. Khoury, "Orbital-angular-momentum mixing in type-II second-harmonic generation," Phys. Rev. A **96**, 053856 (2017).
33. A. Mair, A. Vaziri, G. Weihs, and A. Zeilinger, "Entanglement of the orbital angular momentum states of photons," Nature **412**, 313–316 (2001).
34. D. P. Caetano, M. P. Almeida, P. H. Souto Ribeiro, J. A. O. Huguenin, B. Coutinho dos Santos, and A. Z. Khoury, "Conservation of orbital angular momentum in stimulated down-conversion," Phys. Rev. A **66**, 041801(R) (2002).
35. M. Martinelli, J. A. O. Huguenin, P. Nussenzveig, and A. Z. Khoury, "Orbital angular momentum exchange in an optical parametric oscillator," Phys. Rev. A **70**, 013812 (2004).
36. Z. Zhu, W. Gao, C. Mu, and H. Li, "Reversible orbital angular momentum photon-phonon conversion," Optica **3**, 212–217 (2016).
37. F. Lenzini, S. Residori, F. T. Arecchi, and U. Bortolozzo, "Optical vortex interaction and generation via nonlinear wave mixing," Phys. Rev. A **84**, 061801(R) (2011).
38. N. V. Bloch, K. Shemer, A. Shapira, R. Shiloh, I. Juwiler, and A. Arie, "Twisting light by nonlinear photonic crystals," Phys. Rev. Lett. **108**, 233902 (2012).
39. Z. Zhou, S. Liu, Y. Li, D. Ding, W. Zhang, S. Shi, M. Dong, B. Shi, and C. Guo, "Orbital angular momentum-entanglement frequency transducer," Phys. Rev. Lett. **117**, 103601 (2016).
40. R. W. Boyd, *Nonlinear Optics* (Academic, 2003), p. 96.
41. L. Yu, W. Huang, M. Huang, Z. Zhu, X. Zeng, and W. Ji, "The Laguerre-Gaussian series representation of two-dimensional fractional Fourier transform," J. Phys. A **31**, 9353–9357 (1998).
42. M. J. Padgett and L. Allen, "The Poynting vector in Laguerre-Gaussian laser modes," Opt. Commun. **121**, 36–40 (1995).
43. W. Zhang, Q. Qi, J. Zhou, and L. Chen, "Mimicking Faraday rotation to sort the orbital angular momentum of light," Phys. Rev. Lett. **112**, 153601 (2014).
44. J. Zhou, W. Zhang, and L. Chen, "Experimental detection of high-order or fractional orbital angular momentum of light based on a robust mode converter," Appl. Phys. Lett. **108**, 111108 (2016).
45. X. Fang, Z. Kuang, P. Chen, H. Yang, Q. Li, W. Hu, Y. Lu, Y. Zhang, and M. Xiao, "Examining second-harmonic generation of high-order Laguerre-Gaussian modes through a single cylindrical lens," Opt. Lett. **42**, 4387–4390 (2017).
46. G. Molina-Terriza, J. P. Torres, and L. Torne, "Management of the angular momentum of light: preparation of photons in multidimensional vector states of angular momentum," Phys. Rev. Lett. **88**, 013601 (2002).